Ford Motor Company
AERONUTRONIC DIVISION

(NASA CR-52410 ; ~~Publication No.~~ U-2122)

RESEARCH LABORATORY

FIRST QUARTERLY TECHNICAL REPORT

STRUCTURAL BEHAVIOR OF COMPOSITE MATERIALS

Prepared for: National Aeronautics and Space Administration
Washington, D. C.

Under Contract: NAS-7-215
~~Control No. WOO-PR-63-171~~

Prepared by: S. W. Tsai 24 May 1963 55p refs

Reporting Period: 14 Feb~~ruary~~ - 14 May 1963

24 May 1963

SUMMARY

12952

This report covers the period from February 14 to May 14, 1963. Work was concentrated on (1) theoretical prediction of the composite moduli of unidirectional fiber-reinforced media, and (2) experimental verification of the results. Important aspects are described in this report. Through the week ending May 3, 898 man-hours had been expended; costs that date were $14,665.

AUTHOR

ACKNOWLEDGEMENT

The author wishes to thank his Consultants, Dr. G. S. Springer of Massachusetts Institute of Technology and Dr. A. B. Schultz of the University of Delaware for their contributions and interests in this work.

CONTENTS

ILLUSTRATIONS

SECTION 1

THEORETICAL PREDICTION OF COMPOSITE MODULI

1.1 INTRODUCTION

The unidirectional fiber-reinforced composite considered in this work consists of a large number of filaments embedded with the same orientation in a resin matrix. This composite is treated as a two-phase medium. Similar studies have been undertaken in recent years; in these problems, the composite media were assumed to be locally heterogeneous and grossly homogeneous with the additional specializations:

(1) local and gross isotropy[1,2,3]

(2) local anisotropy and gross isotropy[4].

The present problem is different because the unidirectional composite is locally isotropic and grossly anisotropic. The number of independent moduli increases from two for the grossly isotropic case to four for the present problem. This problem of gross anisotropy has been considered in several earlier studies.[5,6,7,8] Most of these works may be considered modifications of Paul's[1] method since they considered the phases connected in series or in parallel. The proposed solution here relies on more exact mathematical models

and techniques by giving proper consideration to the nature of the mechanical constitutive equation. It will be shown later in this report that the proposed theory is in good agreement with experimental observations.

The description of fiber-reinforced composites has several inherent complications:

(1) The difference in mechanical properties between the two phases is usually large, e.g., 20:1 ratio between Young's moduli. Consequently, any inaccuracy in the theory is magnified. For the same reason, the upper and lower bounds based on Paul's work[1] becomes too far apart to be useful.

(2) Fiber misalignment, as described by catenary K, is the result of process variables.

(3) Photomicrographs revealed that many fibers are in contact, rather than isolated by the matrix. This phenomenon is described by fiber contiguity C. When this is ignored, the measured moduli may fall outside of the theoretically predicted bounds.

The objective of this investigation is to derive the composite anisotropic moduli as functions of the following material and geometric parameters:

$$C_{ij} = C_{ij} (E_f, \nu_f, \rho_f, E_m, \nu_m, \rho_m, R, C, K, \theta) \quad (1)$$

where C_{ij} = composite anisotropic moduli, where $\sigma_i = C_{ij} \epsilon_j$; E = Young's modulus, ν = Poisson's ratio; ρ = specific weight, subscripts f and m refer to the fiber and matrix, respectively; R = percent weight ratio of the matrix; C = contiguity; K = catenary; and θ = fiber orientation.

The derivation of Equation (1) can be simplified considerably by taking advantage of the transformation property of the composite moduli, i.e., Equation (1) can be written as:[9]

$$C_{ij} = C_{ij} (\bar{C}_{ij} \quad \theta) \tag{2}$$

where $\bar{C}_{ij}$ = anisotropic moduli in the elastic symmetry system. Note that $\bar{C}_{ij}$ has only four components instead of six for C_{ij}. Note also that θ is separated out in Equation (2), which is nothing but the transformation equation. Hence the present problem is reduced to:

$$\bar{C}_{ij} = \bar{C}_{ij} (E_f, \nu_f, \rho_f, E_m, \nu_m, \rho_m, R, C, K) \; . \tag{3}$$

Instead of deriving the components of $\bar{C}_{ij}$, it is more convenient to use the engineering constants E_{11} (stiffness parallel to the fibers), E_{22} (stiffness perpendicular to the fibers), ν_{12} (major Poisson's ratio), and G (shear modulus). Again, from the transformation property of $\bar{C}_{ij}$, it can be shown that[9]

$$\begin{aligned} \bar{C}_{11} &= E_{11}/(1 - \nu_{12}\nu_{21}) \\ \bar{C}_{22} &= E_{22}/(1 - \nu_{12}\nu_{21}) \\ \bar{C}_{12} &= \nu_{12}\bar{C}_{22} = \nu_{21}\bar{C}_{11} \\ \bar{C}_{66} &= G \end{aligned} \tag{4}$$

Hence, once the expressions for the four engineering constants in terms of the material and geometric parameters are known, $\bar{C}_{ij}$ and C_{ij} for any value of θ can be computed directly.

1.2 PREDICTION OF E_{11}

The prediction of the composite stiffness parallel to the fibers is based on the well known linear theory that:[1,3,5,6,7,8]

$$E_{11} = E_f - (E_f - E_m)\,\chi \tag{5}$$

where χ = relative volume of matrix = $\dfrac{\rho_f/\rho_m}{\left(\dfrac{100}{R} + \dfrac{\rho_f}{\rho_m} - 1\right)}$.

This theory says that the fibers and the matrix are connected in parallel (Paul's upper bound[1]) and each carries a load proportional to its stiffness. This relation is well confirmed experimentally with the possible exception of a correction for catenary, which can be expressed by an empirical constant K, such that

$$E_{11} = K\left[E_f - (E_f - E_m)\,\chi\right] \tag{6}$$

where $K \leq 1$.

1.3 PREDICTION OF E_{22}

The transverse stiffness of a unidirectional composite can be derived by considering the fibers as parallel cylindrical inclusions, as shown in Figure 1.

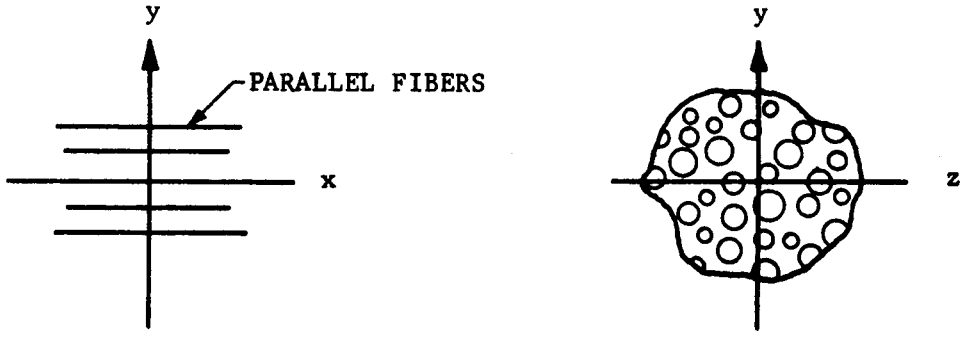

FIGURE 1. UNIDIRECTIONAL COMPOSITE

This problem can be regarded as parallel to Hashin's problem on spherical inclusions.[2] But in the case of high fiber concentration (say χ = 30 percent), many fibers become contiguous, i.e., fibers are in contact rather than isolated by the matrix. Thus, the assumptions in Reference 2 that (1) each inclusion is completely enclosed by the matrix, and (2) the amount of matrix enclosing each inclusion is the same as the average matrix content of the entire composite must be modified. Hence, fiber contiguity must be incorporated in the theoretical prediction of E_{22}.

First, the E_{22} is predicted based on C = 0, i.e., all fibers are isolated and the matrix is contiguous. This has been outlined by the author,[10,11*] where

$$E_{22}^{(m)} = 2\,(1 - \nu_2)\,\frac{K_f(2K_m + G_m) - G_m(K_f - K_m)\,\chi}{(2K_m + G_m) + 2\,(K_f - K_m)\,\chi} \qquad (7)$$

*The derivation of this equation required the application of variational principles to a two-phase composite. This derivation is too lengthy for the present report; thus it is not presented here.

where $E_{22}^{(m)}$ = transverse stiffness for C = 0; $\nu_2 = \nu_f - (\nu_f - \nu_m)\ \chi$ = the Poisson's ratio in the isotropic plane, plane y-z, and is approximated by a linear relation (note ν_2 is not ν_{12}, the major Poisson's ratio of the unidirectional composite); $K_f = E_f / 2\ (1 - \nu_f)$; $G_f = E_f / 2\ (1 + \nu_f)$; $K_m = E_m / 2\ (1 - \nu_m)$; $G_m = E_m / 2\ (1 + \nu_m)$.

The $E_{22}^{(f)}$, the other bound of E_{22} is based on C = 1, where

$$E_{22}^{(f)} = 2\ (1 - \nu_2)\ \frac{K_f(2K_m + G_f) + G_f\ (K_m - K_f)\ \chi}{(2K_m + G_f) - 2\ (K_m - K_f)\ \chi} \quad . \tag{8}$$

This is derived by interchanging subscripts m and f in Equation (7) and replace χ by $(1 - \chi)$.

Finally, the composite E_{22} derived by a linear combination of the two extreme cases:

$$E_{22} = E_{22}^{(m)} + C\ (E_{22}^{(f)} - E_{22}^{(m)}) \tag{9}$$

where $0 \leq C \leq 1$. The actual value of C is expected to be closer to 0 than to 1 because the latter case (the upper bound) replaces the fibers in contact by a contiguous phase of fiber material.

1.4 PREDICTION OF ν_{12}

The major Poisson's ratio can be obtained by considering the isotropic plane in figure 1 in a stste of plane strain, i.e., u = 0 where u is the displacement along x-axis. The amount of axial stress, σ_x, required to maintain u = 0 is proportional to ν_{12}, so that[12]

$$\nu_{12} = \frac{\sigma_x}{\sigma_y + \sigma_z} = \frac{\sigma_x}{2p} \quad . \tag{10}$$

In the case of cylindrical inclusion with C = 0, the contiguous phase (the matrix) forms the outer ring of a concentric cylinder and the dispersed phase (the fiber) the core. Under the influence of hydrostatic pressure, it can be shown that[11]

$$\sigma_r^{(m)} + \sigma_\theta^{(m)} = \frac{2K_m(2K_f + G_m)\, p}{K_m(2K_m + G_m) + G_m(K_f - K_m)\chi} \tag{11}$$

$$\sigma_r^{(f)} + \sigma_\theta^{(f)} = \frac{2K_f(2K_m + G_m)\, p}{K_m(2K_f + G_m) + G_m(K_f - K_m)\chi} \tag{12}$$

where p = hydrostatic pressure, and superscript m and f refer to the outer ring and the core, respectively.

Using Equation (10)

$$\nu_m = \frac{\sigma_x^{(m)}}{\sigma_r^{(m)} + \sigma_\theta^{(m)}}, \qquad \nu_f = \frac{\sigma_x^{(f)}}{\sigma_r^{(f)} + \sigma_\theta^{(f)}} . \tag{13}$$

Following the assumptions in the derivation of E_{11},

$$\sigma_x = \sigma_x^{(m)} + (\sigma_x^{(f)} - \sigma_x^{(m)})\chi . \tag{14}$$

Substitute Equation (11), (12), (13) and (14) into (10)

$$\nu_{12}^{(m)} = \frac{K_f \nu_f (2K_m + G_m)\chi + K_m \nu_m (2K_f + G_m)(1 - \chi)}{K_m(2K_f + G_m) + G_m(K_f - K_m)\chi} \quad . \tag{15}$$

The other bound of ν_{12} for C = 1, i.e., $\nu_{12}^{(f)}$, can be similarly obtained by interchanging subscripts m and f and replace χ by 1 - χ. Hence

$$\nu_{12}^{(f)} = \frac{K_m \nu_m (2K_f + G_f)(1 - \chi) + K_f \nu_f (2K_m + G_f)\chi}{K_f(2K_m + G_f) + G_f(K_m - K_f)(1 - \chi)} \quad . \tag{16}$$

Finally

$$\nu_{12} = \nu_{12}^{(m)} + C(\nu_{12}^{(f)} - \nu_{12}^{(m)}) \quad . \tag{17}$$

1.5 PREDICTION OF G

The transformation equation of the shear modulus is:[9]

$$\frac{1}{G'} = \left(\frac{1}{E_{11}} + \frac{2\nu_{12}}{E_{11}} + \frac{1}{E_{22}} \right) 4m^2n^2 + \frac{1}{G}(m^2 - n^2)^2 \tag{18}$$

where m = cos θ, n = sin θ, and G' = shear modulus of θ fiber orientation. It can be shown that G' reaches a maximum when $\theta = 45^\circ$ by differentiate G' with respect to θ. In fact, at this angle

$$\frac{1}{G_{max}} = \frac{1}{E_{11}} + \frac{2\nu_{12}}{E_{11}} + \frac{1}{E_{22}} \quad . \tag{19}$$

Thus the upper bound of G is established from the transformation equation. Note G_{max} is a function of E_{11}, ν_{12} and E_{22}. Since they depend on C (contiguity) and K (catenary), G_{max} becomes dependent on C and K indirectly. Thus, depending on what combination of C and K values is used, there will be one absolute upper bound (when C=K=1) and many relative upper bounds for G.

The lower bound of G is derived by chopping the continuous fibers and reshaping the segments into spheres. Hence the solution of the composite shear modules for a medium with spherical inclusions[2] becomes applicable. Since shear modulus is associated with the resistance to distortion, a composite with spherical inclusions is intuitively less rigid than one with cylindrical inclusions; this justifies the use of the spherical composite for the lower bound of G. Hence, from Reference 2,

$$G^L = G_m + \frac{15\,(1-\nu_m)\,(\frac{G_f}{G_m}-1)\,(1-\chi)\,G_m}{7-5\,\nu_m + 2\,(\Delta - 5\,\nu_m)\,[\,1+(\frac{G_f}{G_m}-1)\chi]} \qquad (20)$$

where G^L = lower bound of G. Thus, the shear modulus of a unidirectional composite must satisfy:

$$G_{max} \geq G \geq G^L$$

where G_{max} and G^L are computed from Equations (19) and (20), respectively.

SECTION 2

EXPERIMENTAL PROCEDURE AND SPECIMEN PREPARATION

2.1 EXPERIMENTAL PROCEDURE

The experimental determination of the anisotropic constants was obtained in accordance with the procedure outlined in Appendix A. All moduli were measured by flexural and twisting tests.

To ascertain the accuracy of the test method, a number of simple tests were performed for the purpose of comparison and calibration. These tests will now be discussed.

a. Specimen Size and Gage Length

A series of tests was run to determine the proper specimen size and gage length for the plate and beam specimens. The thickness of the specimen ran from 0.1 to 0.2 inch. Five-inch square plate specimens were used for the twisting tests in the present program, since below 5 inches, the apparent shear moduli was higher than the actual. The beam specimens were 3/4-inch to 1-inch wide. For central load flexural test, 6-inch span provided

accurate data. Shorter spans yielded lower apparent stiffness. For double load flexural test, the long span was 8 inches and short span 4 inches. The test was not used extensively because longer specimens (8 inches instead of 6 inches) were needed; simultaneous contact between the loading points and the beam was difficult to achieve; thus, higher deflection often becomes necessary. The results obtained from both central and double load tests on the same specimen were identical.

b. Tensile and Flexural Stiffnesses

The interpretation of test data using the bending theory of plates and beams (strength of materials) was checked against (1) simple tensile test with extensometer; (2) simple tensile with strain gages; and (3) double load flexural with strain gages. Results indicated that for strain up to 0.2 percent, there was no appreciable difference ($<$ 10 percent) between the stiffnesses measured by tensile and flexural tests. Close agreement also existed between the surface strain predicted by the simple beam theory and the direct reading from the strain gages. Planes apparently remained planes for 0 and 90-degree beams. There was no shift in the neutral axis (strain recordings on both sides of the beam were identical). The implication was that tensile, compressive, and flexural moduli, at least for E_{11} and E_{22}, were essentially the same.

2.2 UNIDIRECTIONAL SPECIMENS

Three systems of unidirectional specimens were made. In all cases, unidirectional plies were laid by hand to provide the final thickness. Resin

content for each system represents the average of four samples taken from widely spaced locations.

a. SP-1

This system consisted of 20 plies of Minnesota Mining and Manufacturing Company Scotch-ply #1009-33 W2 38. The curing cycle was: press preheated to 200°F, pressure 40 psi, temperature 300°F for 2 hours, followed by slow cooling. Cured thickness was 0.18 inch and resin content 23 percent.

b. X_b

This system consisted of 11 plies of U. S. Polymeric Company E-787-NUF. The curing cycle was: no preheat, pressure 50 psi, temperature 300°F for 2 hours, followed by slow cooling. Cured thickness was 0.20 inch and resin content 16 percent.

c. XVII

This system was the same as X_b above, except the resin content was 15 percent.

SECTION 3

EXPERIMENTAL VERIFICATION

In this section, the theoretical predictions as outlined in Section 1 are compared with experimental measurements. Only glass filament-epoxy resin systems with the following properties were used:

$$E_f = 10.6 \times 10^6 \text{ psi}$$
$$\nu_f = 0.22$$
$$\rho_f = 2.60$$
$$E_m = 0.5 \times 10^6 \text{ psi} \qquad (21)$$
$$\nu_m = 0.35$$
$$\rho_m = 1.15$$

3.1 AXIAL STIFFNESS E_{11}

Substituting the data in Equation (21) into Equation (6), E_{11} for K = 1 and 0.9 were computed and shown in Figure 2. Experimental points are also shown. Note that SP-1 and data from Reference 3 agree with the K = 1. case, while X_b and XVII agree with K = 0.9. A visual examination of X_b and XVII (the NUF Systems) revealed that the filaments were less straight. This

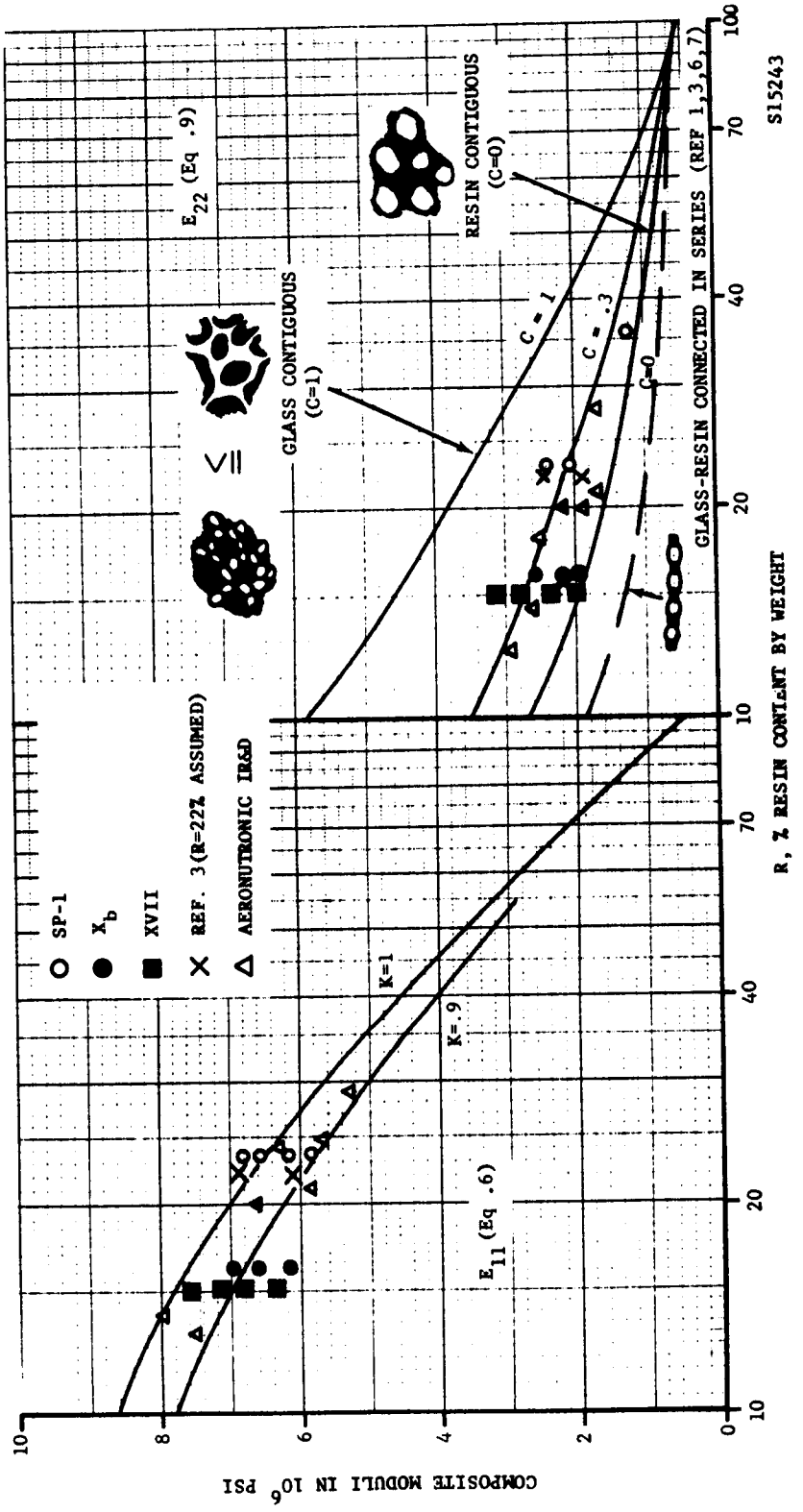

FIGURE 2. E_{11} AND E_{22} VERSUS R

resulted partially from the periodic cross ties (transverse to the fibers). Thus, the assumed catenary seemed reasonable.

3.2 TRANSVERSE STIFFNESS E_{22}

Using the same data of Equation (21), E_{22} was computed from Equation (9) for C = 0, 0.3, and 1. These are also shown in Figure 2. It appeared that experimental data agreed with the case of C = 0.3. Note that catenary did not affect E_{22}. This was in agreement with the theory, Equation (9). The E_{22} predicted by References 1, 3, 6, 7 was also shown. This curve was obtained by considering the two phases connected in series. It was clear that this prediction yielded considerably lower values than those measured.

The contiguity factor C though convenient and good in theory, still needed a more critical verification. For this reason, steel rod-epoxy composites were made with C = 0, i.e., each rod was completely separated by the resin. The specimen preparation and test procedure and results are shown in Appendix B. Substituting the following data:

$$E_f = 30 \times 10^6 \text{ psi}$$

$$\nu_f = \nu_m = 0.30$$

$$\rho_f = 7.80 \qquad (22)$$

$$E_m = \text{as measured, i.e., } 0.46, 0.43, 0.59 \times 10^6 \text{ psi}$$

$$\rho_m = 1.15$$

into Equation (9) for C = 0, 0.3, and 1, the computed results and the data from Appendix B are shown in Figure 3. It is seen that the data agreed with the

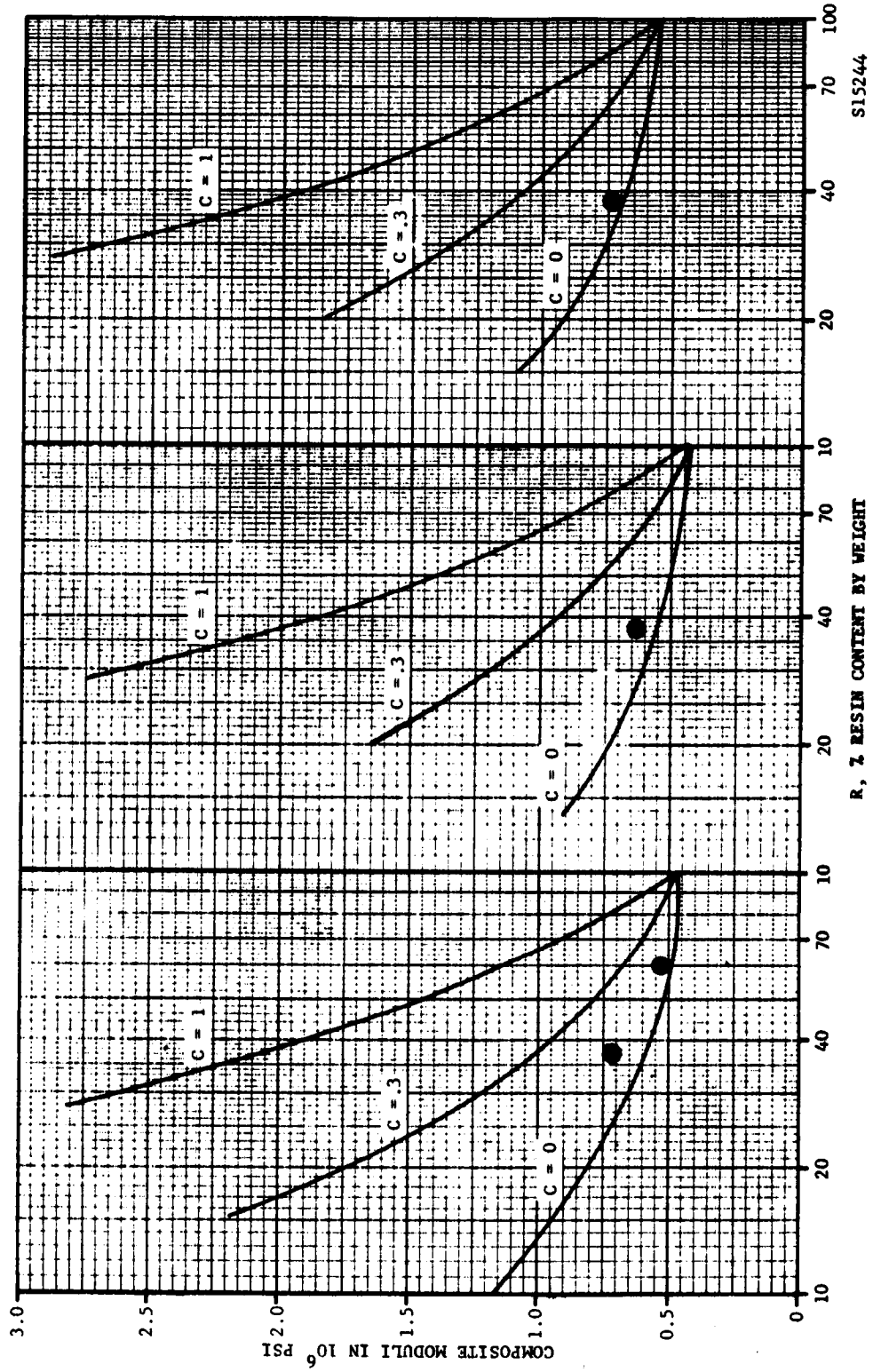

FIGURE 3. E_{22} OF STEEL-EPOXY COMPOSITES

C = 0 case very well. This result may be considered a partial verification of the significance of contiguity.

3.3 MAJOR POISSON'S RATIO ν_{12}

Using the data of Equation (21), ν_{12} was computed from Equation (17) for C = 0, 1. This is shown in Figure 4, together with the measured points. It is seen that the SP-1 point and the Aeronutronic IR & D points agreed with the theory and satisfied C = 0.3 approximately, whereas X_b and XVII have large spreads. Possible explanations of this poor agreement may be (1) the actual values of ν_m and ν_f were different from those used in Equation (21); or (2) more importantly, C_{12} of Equation (4) is small in comparison with C_{22}; hence, any error in E_{22} is magnified in ν_{12}. The wide scatter of E_{22} for the NUF systems (X_b and XVII) as shown in Figure 2 induced the even wider scatter in ν_{12}.

3.4 SHEAR MODULUS G

Again using the data on Equation (21), Equations (19) and (20) were solved for C = 0, 0.3 and 1, and K = 1 and 0.9. This is also shown in Figure 4. Since K = 1 for SP-1, K = 0.9 for X_b and XVII, two separate diagrams were drawn with the applicable measured points plotted. The bounds based on Paul's theory[1] were drawn in dotted lines to illustrate the inaccuracy of this approximate theory when E_f is much greater than E_m.

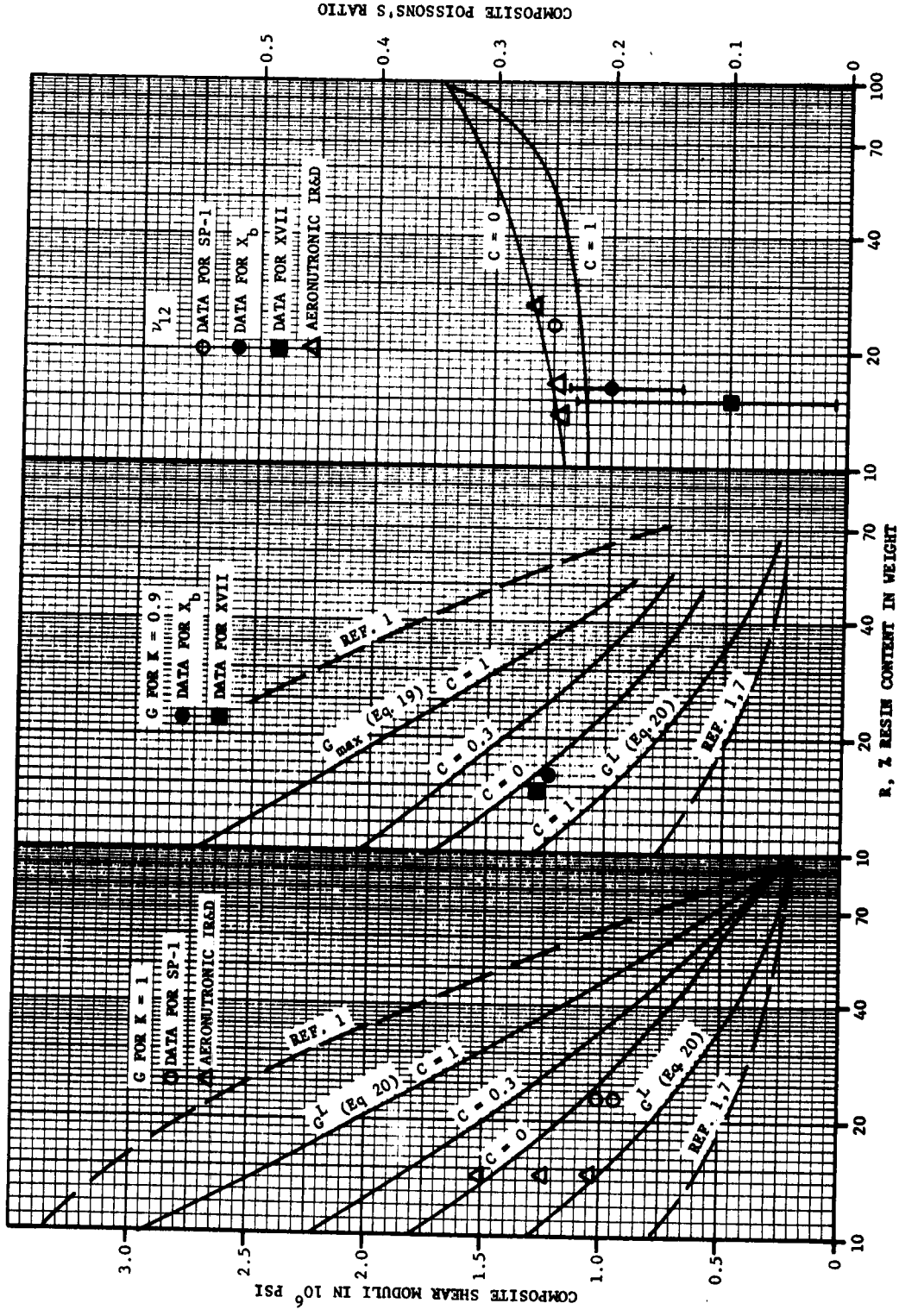

FIGURE 4. ν_{12} AND G VERSUS R

For a given K value (1 or 0.9), the absolute upper bound for G would be the case when C = 1. Since for the particular glass-epoxy system the observed C value is approximately 0.3, it is reasonable to use the C = 0.3 case as the upper bound of G. From Figure 4, it is seen that the present theory lowers Paul's upper bound by a substantial margin.

The lower bound of G based on Equation (20) is also higher than Paul's lower bound. Thus the gap between the bounds has been narrowed. The lower bound of G can be raised if the contiguity of the spherical inclusions is taken into consideration, in the same way as the contiguity of the cylindrical inclusions in a unidirectional composite. One will then obtain relative lower bounds for various values of contiguity, while Equation (20) remains as the absolute lower bound.

It should be emphasized that the upper and lower bounds of G were derived from entirely different mathematical models. But these curves as functions of resin contents have approximately the same shape. So, as an approximation, the case of C = 0 for E_{22} in Equation (19) may be regarded as the approximate G curve. This agreed with the experimental value for glass-epoxy systems.

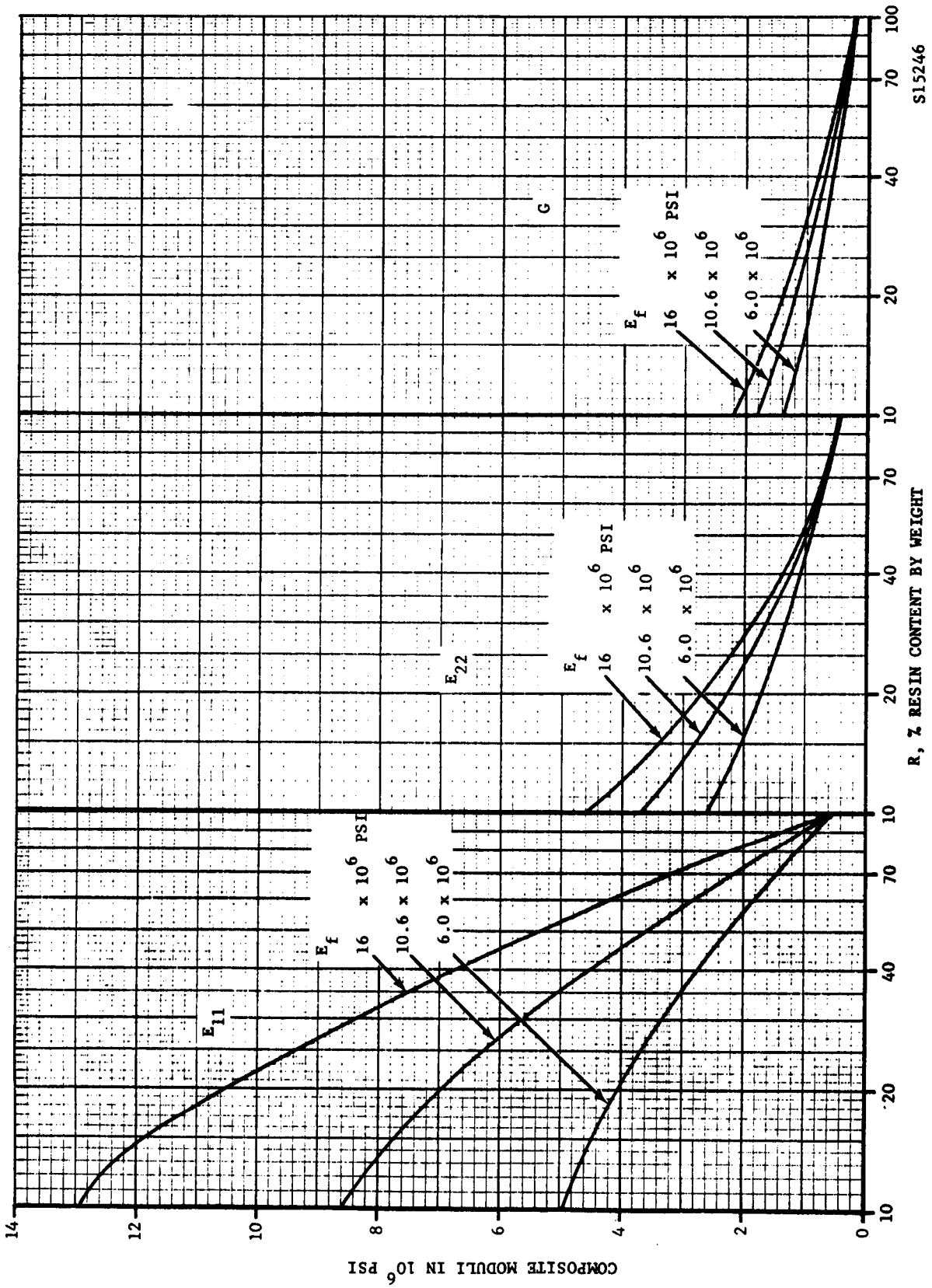

FIGURE 5. CONTRIBUTION OF E_f TO E_{11}, E_{22} AND G

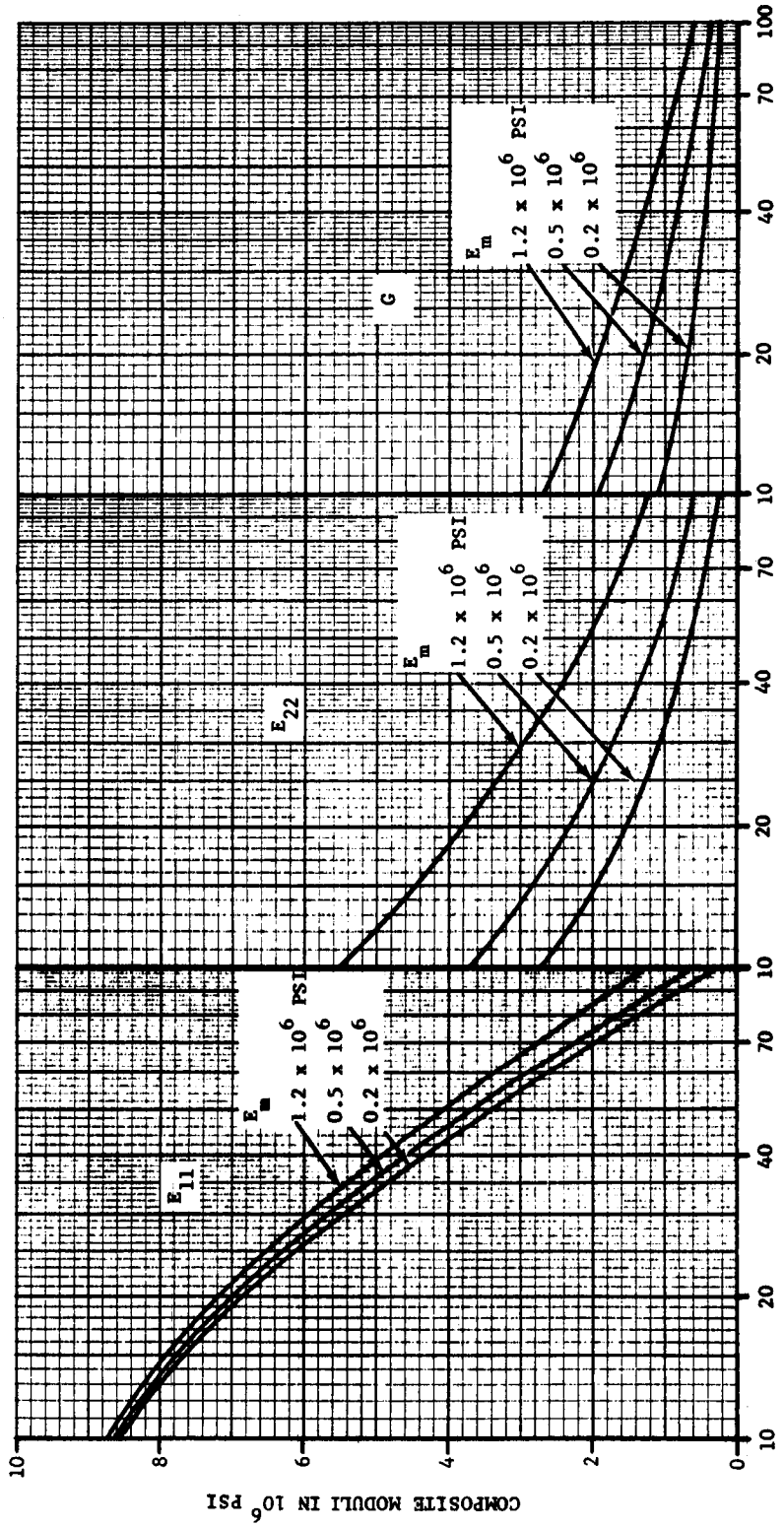

FIGURE 6. CONTRIBUTION OF E_m TO E_{11}, E_{22} AND G

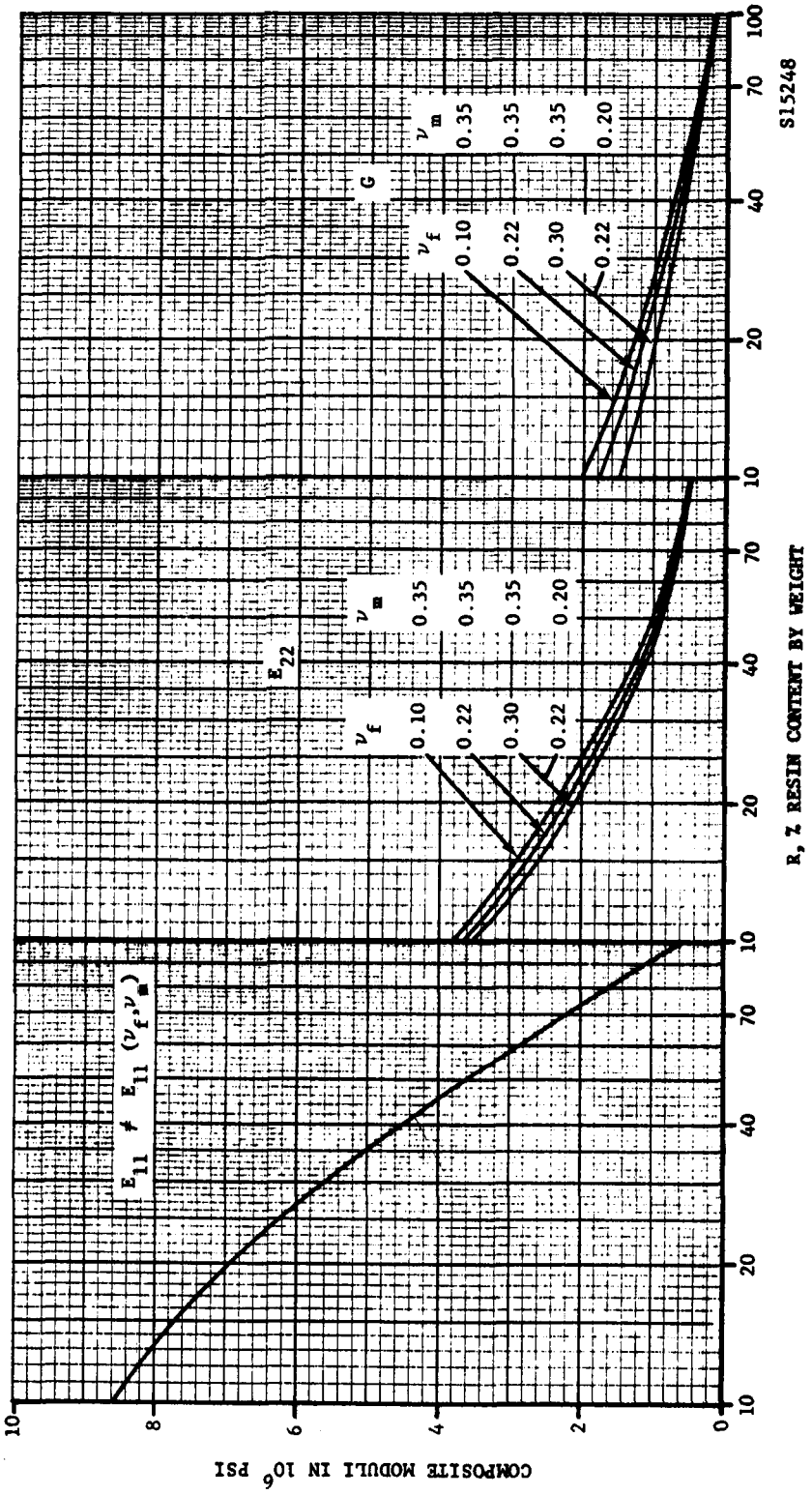

FIGURE 7. CONTRIBUTION OF ν_m AND ν_f TO E_{11}, E_{22} AND G

SECTION 4

CONCLUSIONS AND FUTURE PLAN

4.1 CONCLUSIONS

The progress to date indicated that the basic theoretical predictions of the composite moduli of unidirectional fiber-reinforced composites were in agreement with experimental observations. Needless to say, further refinement of the theory will be made when more facts become available.

Based on the present theory, the contribution of each material parameter to the composite moduli can be predicted. This is shown in the following figures:

Figure 5: E_{11}, E_{22}, and G versus E_f

Figure 6: E_{11}, E_{22}, and G versus E_m

Figure 7: E_{22} and G versus ν_f and ν_m

In all the curves, the middle curve was computed from the data of Equation (21), which is a representative E-801 glass-epoxy system. Other variations reflected fictitious materials, with the exception of $E_f = 16.0 \times 10^6$ psi which is a representative high modulus glass. For all cases, C = 0.3 and K = 1 were maintained. G is computed with E_{22} of C = 0 in Equation (19).

From the above, the following may be concluded:

(1) E_f makes significant contribution to E_{11}.

(2) E_m makes significant contribution of E_{22} and G.

(3) ν_f and ν_m do not make significant contributions to E_{11}, E_{22}, and G. For this reason, variation of ν_{12} has not been investigated.

Insofar as geometric parameters, R, C and K are concerned, one can conclude:

(1) Resin content R makes significant contribution to E_{11}, E_{22}, and G as shown in curves above.

(2) Contiguity C is probably not a controllable parameter for the system under investigation. Insofar as stiffness is concerned, higher value of C increases E_{22}. This effect, however, may be detrimental to the strength of the composite. It is also of interest to note that when the E_f and E_m are of the same order of magnitude the bounds based on contiguity become very close. This is shown on Figure 8 computed for $E_f = 16 \times 10^6$ psi, $\nu_f = 22$, $E_m = 5.0 \times 10^6$, $\nu_m = 0.35$. This may be considered as a justification for ignoring contiguity in Hashin's work,[2] in which $E_f/E_m = 3.4$.

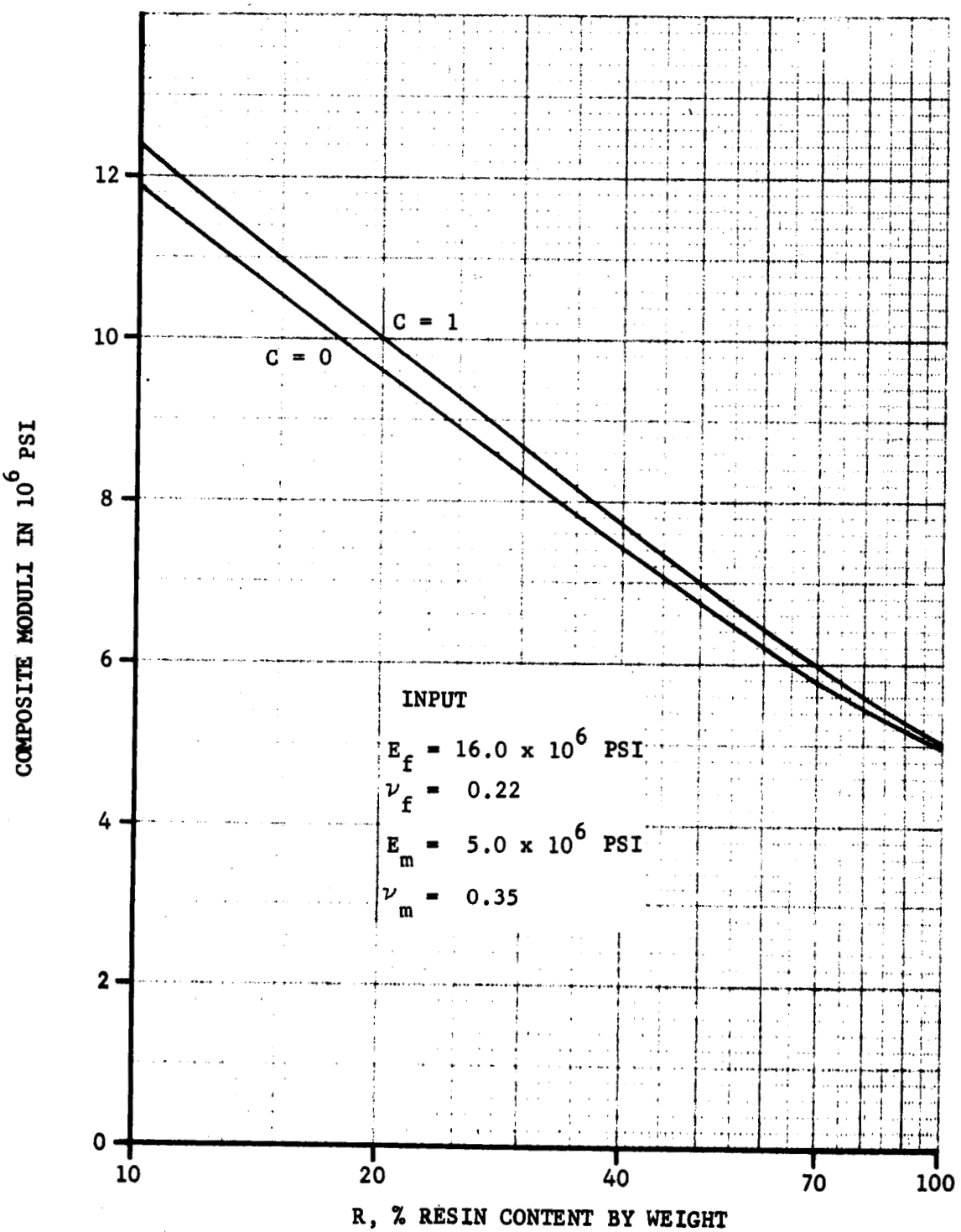

FIGURE 8. E_{22} VERSUS R FOR C = 0 AND 1

(3) Catenary K affects not only E_{11} but G as well. This is detrimental in the sense that it decreases both E_{11} and G. Again, no speculation of this effect on strength can be made at this time.

4.2 FUTURE PLAN

Further experimental verification of unidirectional system will be performed. Specifically, two systems will be investigated: (1) high modulus glass ($E_f = 16 \times 10^6$ psi) with regular epoxy; and (2) regular glass with a soft matrix ($E_m = 0.25 \times 10^6$ psi). This will conclude the work on the unidirectional system.

The next phase will be concerned with the effect of lamination of unidirectional systems. Two types of laminated constructions will be investigated theoretically, then verified experimentally.

a. Cross-ply System

Two geometric parameters will be investigated: (1) total number of plies, N; and (2) the cross-ply ratio, M, which is the ratio of the combined thickness of one unidirectional system over that placed orthogonal to it.

b. Angle-ply System

Two geometric paramets will be investigated: (1) N, same as above; and (2) angles of fiber orientations, θ. Only symmetrically oriented systems will be investigated.

REFERENCES

1. B. Paul, "Prediction of Elastic Constants of Multi-phase Materials," Trans. AIME, Vol. 218, 1960, pp 36-41.

2. Z. Hashin, "The Elastic Moduli of Heterogeneous Materials," J. App. Mech., March 1962, pp 143-150.

3. D. P. Hanley and R. F. H. Woodberry, "Highlights of Other ABL Sponsored Research Investigations," Proc. Fourth Semiannual Polaris Glass Reinforced Plastic R & D Conference, January 1963.

4. Z. Hashin and S. Shtrikman, "On Effective Elastic Moduli of Multiphase Materials and Polycrystals," Proc. of Fourth U. S. National Congress of Applied Mechanics, June 1962, pp 619-625.

5. O. Hoffman, "Stresses and Deformations in Filament-Reinforced Structures," IAS paper #62-26, January 1962.

6. F. Beer, "Die Festigkeitseigenschaften Kreuzweise bewehrter Kunstoffe," VDI-Z, Vol. 101, April 1959, pp 463-468.

7. J. T. Hofeditz, "Structural Design Considerations for Fiber Glass Pressure Vessels," Proc. 18th Annual Technical and Management Conference - Reinforced Plastic Division, Soc. Plastic Industry, February 1963, Sect. 7-C.

8. W. T. Walker, "Material Design Properties for Filament-Wound Construction," Proc. Fourth Semiannual Polaris Glass Reinforced Plastic R & D Conference, January 1963.

9. S. G. Lekhnitzkiy, "Anisotropic Plates," 2nd Ed., Moscow, 1957.

10. S. W. Tsai, "A Variational Formulation of Two-Dimensional Heterogeneous Media," Aeronutronic Publ. #U-1698, June 1962.

11. S. W. Tsai, "Composite Stiffnesses of Fiber-Reinforced Media," Aeronutronic Publ. #U-1699, June 1962.

12. S. Timoshenko and J. N. Goodier, "Theory of Elasticity" 2nd Ed., New York, 1951.

APPENDIX A

EXPERIMENTAL DETERMINATION OF THE ELASTIC BEHAVIOR OF ANISOTROPIC PLATES AND SHELLS

INTRODUCTION

In modern technology, severe loading and environmental conditions coupled with the consideration of weight have dictated the use of many non-isotropic and non-homogeneous materials, examples of which include the pyrolytic graphite, reinforced plastics, fiber-reinforced composites, and filament-wound materials. A thorough understanding of anisotropic elasticity becomes a pre-requisite among the materials and structural engineers of this field. Since material response to external loads depends entirely on the stress-strain relation of the material, accurate determination of the coefficients of this relation, i.e., the anisotropic elastic constants, is of fundamental importance in the description of the elastic behavior of a given material.

ANISOTROPIC PLATES AND SHELLS

In order to facilitate ensuing discussions, all relevent terminology and relations will now be covered.

As mentioned above, the elastic behavior of a two-dimensional anisotropic body is described by the following stress-strain relation

$$\epsilon_i = s_{ij} \sigma_j \qquad (1)$$

where ϵ_i = strain components; σ_j = stress components; s_{ij} = compliance matrix. In the contracted notation, i, j = 1, 2, 6, where 1, 2 refer to the normal components and 6 to the shear component of stress and strain..

1-2 also designate x-y, z - θ, and ϕ - θ. for rectangular, cylindrical and spherical coordinates, in that order.

The compliance matrix is symmetric, thus there are in general six different components. If the elastic symmetry axes X - Y coincide with the reference coordinates, shown as x - y in Figure A-1, $s_{16} = s_{26} = 0$. This special symmetry is called orthotropic and is designated by S_{ij}, which has only four independent components. The stress-strain relation reduces to:

$$\epsilon_x = X_{11}\ \sigma_x + S_{12}\ \sigma_y$$

$$\epsilon_y = S_{12}\ \sigma_x + S_{22}\ \sigma_y \qquad (2)$$

$$\gamma_{xy} = S_{66}\ \tau_{xy}$$

Since the compliance matrix is a fourth rank tensor, S_{ij} and s_{ij} are related by the following transformation equations:

$$s_{11} = m^4\ S_{11} + 2m^2n^2\ S_{12} + n^4\ S_{22} + m^2n^2\ S_{66} \qquad (3)$$

$$s_{12} = m^2n^2\ S_{11} + (m^4 + n^4)\ S_{12} + m^2n^2\ S_{22} - m^2n^2\ S_{66} \qquad (4)$$

$$s_{22} = n^4\ S_{11} + 2\ m^2n^2\ S_{12} + m^4\ S_{22} + m^2n^2\ S_{66} \qquad (5)$$

$$s_{66} = 4\ m^2n^2\ S_{11} - 8\ m^2n^2\ S_{12} + 4\ m^2n^2\ S_{22} + (m^2-n^2)^2\ S_{66} \qquad (6)$$

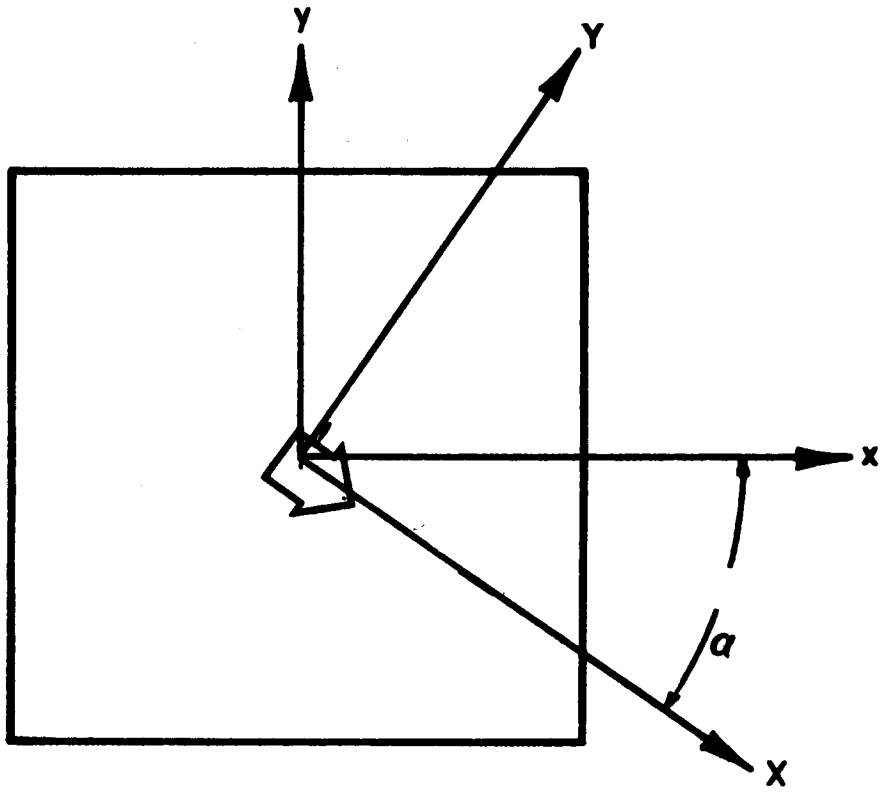

S15250

FIGURE A-1. RELATION BETWEEN COORDINATE AXES X - Y AND ELASTIC SYMMETRY AXES X - Y

$$s_{16} = -2\,m^3n\,S_{11} + 2\,(m^3n-mn^3)\,S_{12} + 2\,mn^3\,S_{22} + (m^3n-mn^3)\,S_{66} \quad (7)$$

$$s_{26} = -2mn^3\,S_{11} + 2\,(mn^3-m^3n)\,S_{12} + 2\,m^3n\,S_{22} + (mn^3-m^3n)\,S_{66} \quad (8)$$

where $m = \cos\alpha$ and $n = \sin\alpha$. Thus knowing the four independent components of S_{ij} in (2), one can compute s_{ij} for all orientations of X - Y axes, i.e., all values of α. It should be obvious that the determination of elastic behavior of anisotropic plates and shells is more easily achieved by measuring the components of S_{ij} than s_{ij}.

EXISTING METHODS

Existing methods in the determination of S_{ij} involve three steps:

1) Bending of a 0°-rectangular plate, i.e., $\alpha = 0^\circ$, from which S_{11} and S_{12} are measured;
2) Bending of a 90°-rectangular plate, i.e., $\alpha = 90^\circ$, from which S_{22} and S_{12} are measured; and
3) Twisting of a 0°-square plate, from which S_{66} is measured.

The loading scheme of imposing a uniformly distributed bending moment along two opposite edges of a plate was first proposed by Bergstrasser,[1] intended to measure simultaneously the Young's modulus and Poisson's ratio of an isotropic plate. This scheme required a long rectangular plate be bent by six different forces, different in direction and magnitude, with

each located at a predetermined position. This complicated scheme is necessary because the deflected surface is anti-synclastic. Hearmon and Adams[2] applied this bending scheme to anisotropic plates (ply-wood). Witt, et al.[3] improved this technique by using a different loading fixture. The accuracy of this bending test depends on the length-to-width ratio of the test section of the plate specimen. In the last two references, this ratio was unity, which was very small. At the same time, the absolute dimension of the width of the plate must also be large to insure a good measurement of S_{12}. These two requirements together demand a large size specimen and this induces numerous experimental difficulties--availability of materials, and testing machines, geometric and material uniformity, machining and handling, instrumentation, etc.

The twisting test, on the other hand, is theoretically sound because it has an "exact" load-moment relation. The loading scheme is extremely straight forward in principle, applying equal loads to all the corners of a square plate, with the loads in the first and third quadrants upward and in the second and fourth downward. In references [2] and [3] the specimens used were limited to the 0^{o}-plates. The loading scheme, in all three references, called for two fixed supports and two loading points. This is also difficult to carry out experimentally, and will be seen later.

PROPOSED METHOD

Recognizing the theoretical limitation on the load-moment relation of the bending test and the experimental difficulties of both the

bending and twisting tests, a method is presented to show that reliable data on the elastic behavior of anisotropic materials can be obtained.

First of all, the bending of plate specimens is discarded. Instead of plates, beams will be used so that the standard beam flexural test can be used. In addition, only one type of beam, 0° or 90°, is required.

Secondly, the pure twisting test will be applied to both the 0°- and 45°-plates. It will be shown later that sufficient data can be obtained for the complete determination of the independent constants.

Thirdly, the loading scheme of the pure twisting test, as shown in Figure A-2, has three fixed and one loading points, instead of two fixed and two loading points. This improvement insures the necessary load distribution while maintaining a fixed reference coordinate system, i.e, the plate specimen cannot have rigid-body motion. What is equally important is that this scheme readily permits direct load-deflection recording by standard testing machines.

Thus, the proposed method is more accurate in theory and simpler to perform than existing methods. More reliable data can be expected.

PURE TWISTING TEST

The proposed method puts more emphasis on the pure twisting test. This will be discussed in detail in this section.

The solution of the differential equations of an anisotropic plate under homogeneous moments, as shown in [2] and [3], is

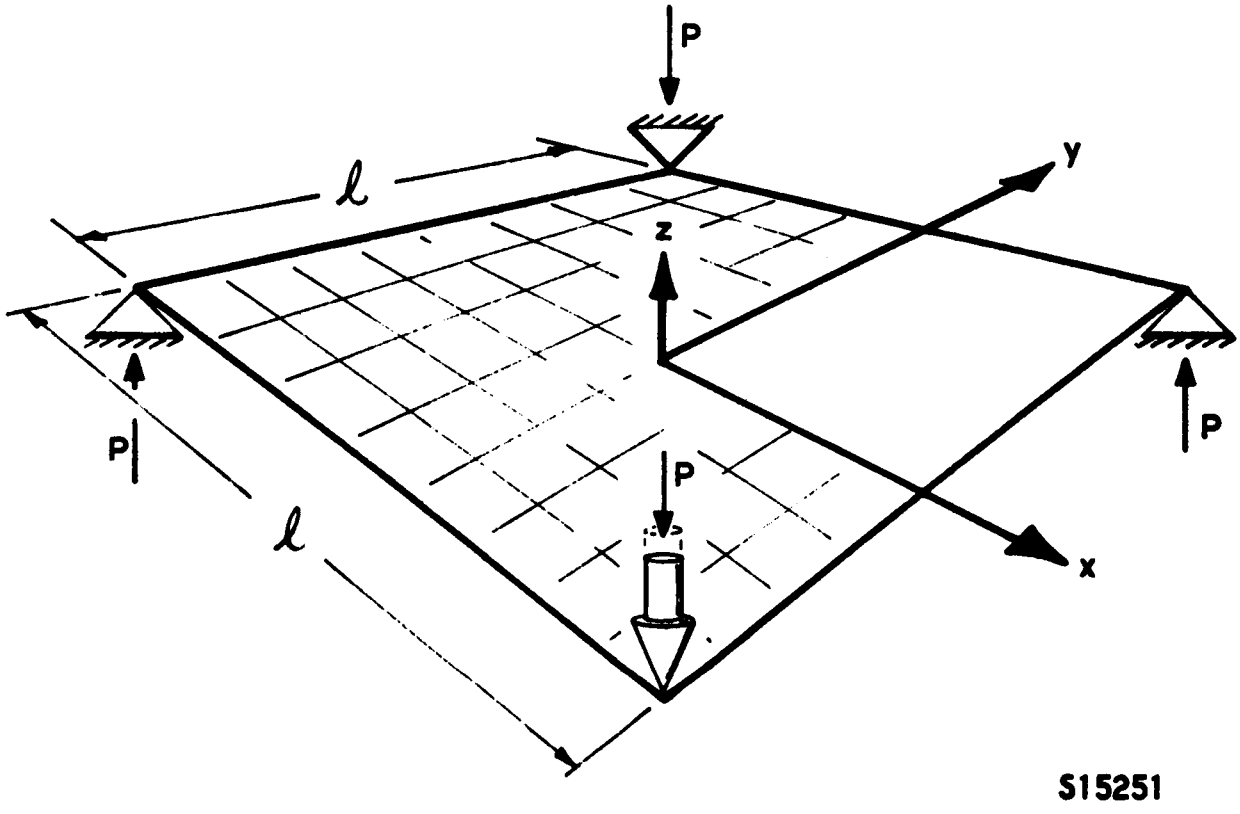

FIGURE A-2. LOADING SCHEME FOR PURE TWISTING TEST

$$
\begin{aligned}
h^3 w = {} & 6 M_x (s_{11} x^2 + s_{12} y^2 + s_{16} xy) \\
& + 6 M_y (s_{21} x^2 + s_{22} y^2 + s_{62} xy) \\
& + 6 M_{xy} (s_{61} x^2 + s_{62} y^2 + s_{66} xy) \\
& + a x + b y + c
\end{aligned}
\tag{9}
$$

where h = plate thickness; w = transverse deflection (along z-axis); M_x, M_y, M_{xy} = bending and twisting moments; a, b, c = constants depended on the position of the reference coordinates.

A plate loaded as shown in Figure 2 is subjected to a homogeneous twisting moment that

$$M_{xy} = -P/2, \; M_x = M_y = 0 \tag{10}$$

Hence (9) reduces to:

$$h^3 w = -3 P (s_{61} x^2 + s_{62} y^2 + s_{66} xy) + ax + by + c \tag{11}$$

In the case when the corners of the plate in the first, second and third quadrants are supported by fixed points, then

$$
\begin{aligned}
w = 0 \text{ when } & x = \ell/2, \; y = \ell/2 \\
& x = \ell/2, \; y = \ell/2 \\
\text{and } & x = -\ell/2, \; y = -\ell/2
\end{aligned}
\tag{12}
$$

Substitute these boundary conditions in (11), and solve for constants a, b and c, then (11) becomes

$$h^3 w = -3P\left[(x^2 - \ell^2/4)\, s_{61} + (y^2 - \ell^2/4)\, s_{62} + (xy - x\,\ell/2 + y\,\ell/2 + \ell^2/4)\, s_{66}\right] \tag{13}$$

Note that the deflection at the center of the plate is

$$h^3 w_o = 3P\ell^2 (s_{61} + s_{62} + s_{66})/4 \tag{14}$$

or
$$S_G = s_{61} + s_{62} + s_{66} = 4h^3 w_o / 3P\ell^2 \tag{15}$$

Thus, the pure twisting test will yield S_G, the sum of the three elastic constants, S_{61}, S_{62} and S_{66}. From (6), (7) and (8), one obtains

$$S_G = -2mn(m-n)^2 S_{11} - 8m^2n^2 S_{12} + 2mn(m+n)^2 S_{22} + (m^2 - n^2)^2 S_{66} \tag{16}$$

Note when
$$\begin{aligned} \alpha &= 0, & S_G &= S_{66} \\ \alpha &= +45^\circ, & S_G &= 2(S_{22} - S_{12}) \\ \alpha &= -45^\circ, & S_G &= 2(S_{11} - S_{12}) \\ \alpha &= \pm 90^\circ, & S_G &= S_{66} \end{aligned} \tag{17}$$

It is clear that by using 0° and 45°-plates, which gives $\alpha = 0$ and 90°, and $\alpha = \pm 45^\circ$, respectively, one obtains three equations for the four

unknown constants. With the data from the beam test, one obtains the fourth equation--either the 0^{o}- or 90^{o}-beam, which yields S_{11} or S_{22}, respectively. Note that only one bending test is necessary.

Also note that the deflection at the loading corner, where $x = \ell/2$, $y = \ell/2$, gives direct measurement of s_{66}. Substitute this location in (13) and rearrange:

$$S_{66} = h^3 w_L / 3 P \ell^2 \qquad (18)$$

where w_L = deflection at the loading corner. Although s_{66} is not a required measurement for the determination of the independent constants, it is a by-product of the pure twisting test. This can be used to check the accuracy of the proposed method.

EXPERIMENTAL VERIFICATION

In order to demonstrate the validity and accuracy of the proposed method, the determination of the elastic constants of an anisotropic plate was performed.

The specimens were made of Minnesota Mining and Manufacturing Company's unidirectional "Scotch-ply", which consisted of glass filaments imbedded in an epoxy resin matrix. The resin content by weight was 23 percent. The plate thickness was approximately 0.2 inch. The assumed homogeneity of the composite material was reasonable because there are hundreds of filaments across the plate thickness. This type of material machines very easily. Thus it is a good test material for anisotropic plate.

The bending test on beams was the standard central-loading flexural test. The pure twisting test was accomplished with a very simple test fixture, which provided three fixed supports in the first, second and third quadrants, with the directions indicated in Figure 2. The remaining corner, in the fourth quadrant, was the loading point by the Instron testing machine. Direct recording of load and the vertical displacement of the loading point, i.e., P and w_L in (18) was obtained. The displacement of the center of the plate, w_o in (15), was read from a dial gage and recorded directly by "pipping" the Instron recorder. Thus from the same chart, both P/w_L and P/w_o were derived.

From the central-loading flexural test of three 0^o-beams, the average compliance was:

$$S_{11} = .16 \times (10^6 \text{ psi})^{-1} \tag{19}$$

From the pure twisting test of 0^o- and 45^o-square plates, the following were obtained by using (17):

$$\begin{aligned} S_{66} &= 1.10 \times (10^6 \text{ psi})^{-1} \\ S_{11} - S_{12} &= .20 \times (10^6 \text{ psi})^{-1} \\ S_{22} - S_{12} &= .57 \times (10^6 \text{ psi})^{-1} \end{aligned} \tag{20}$$

S_{12} and S_{22} were then computed by combining (19) and (20) so that,

$$S_{12} = -.04 \times (10^6 \text{ psi})^{-1}$$
$$S_{22} = .53 \times (10^6 \text{ psi})^{-1} \qquad (21)$$

By bending 90°-beams, the resulted S_{22} was $.50 \times (10^6 \text{ psi})^{-1}$. This was a good independent check of the S_{22} derived in (21).

Knowing the four independent elastic constants, one can readily compute from (3) through (8) the theoretical elastic constants for other orientations. These constants, of which there are six, are plotted in Figure A-3. Note that s_{22} and s_{26} curves are not drawn explicitly because they are the mirror image of s_{11} and s_{16}, respectively. The plane of reflection is at $\alpha = 45^\circ$.

As stated before, the present test procedure furnishes readily independent check of the results obtained above. Three additional square plates were made and tested. The orientations were 15°, 22.5°, and 30°. From these plates, s_{66} and S_G for six different orientations were obtained. These data compared favorably with the theoretical results computed from the four independent constants. This is shown on Figure A-4. The average deviation between the theoretical and experimental points is about 5 percent. For this particular test specimen, better verification than 5 percent would be hard to achieve because geometric and material variation of the specimens amounted to almost the same order of magnitude.

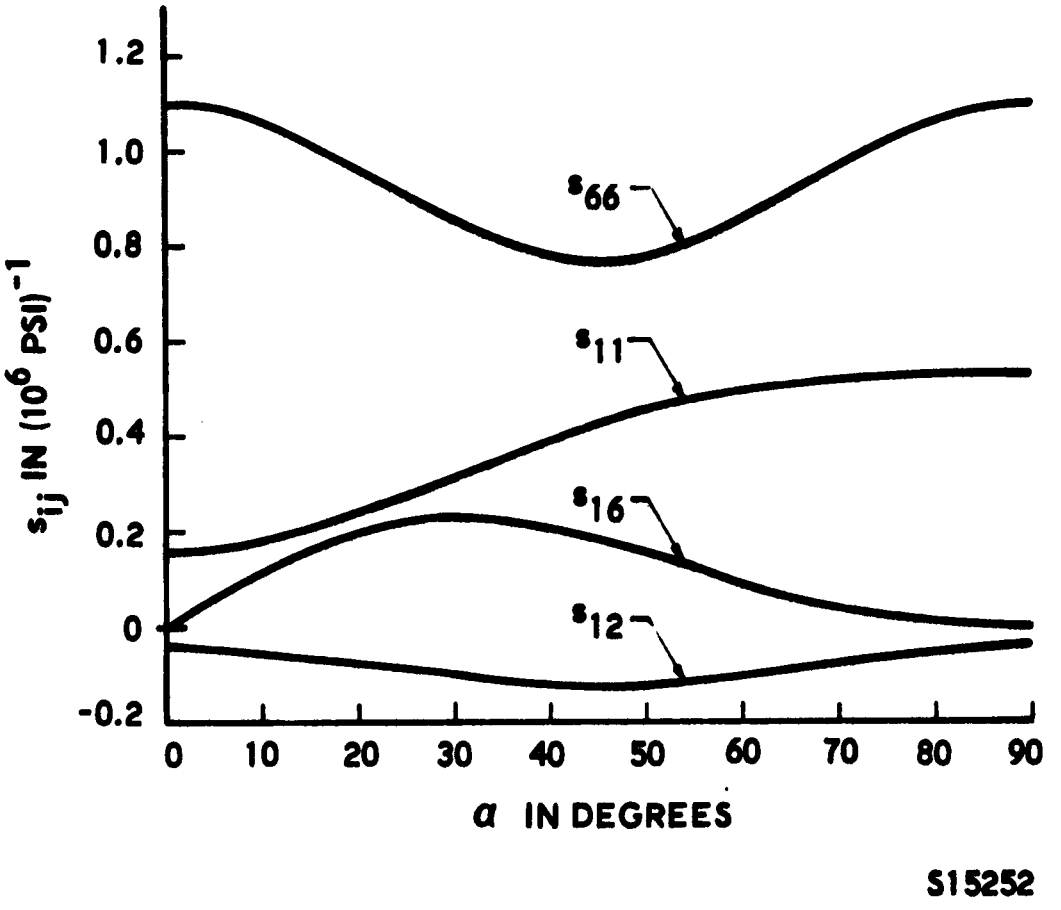

FIGURE A-3. TRANSFORMATION OF S_{ij}

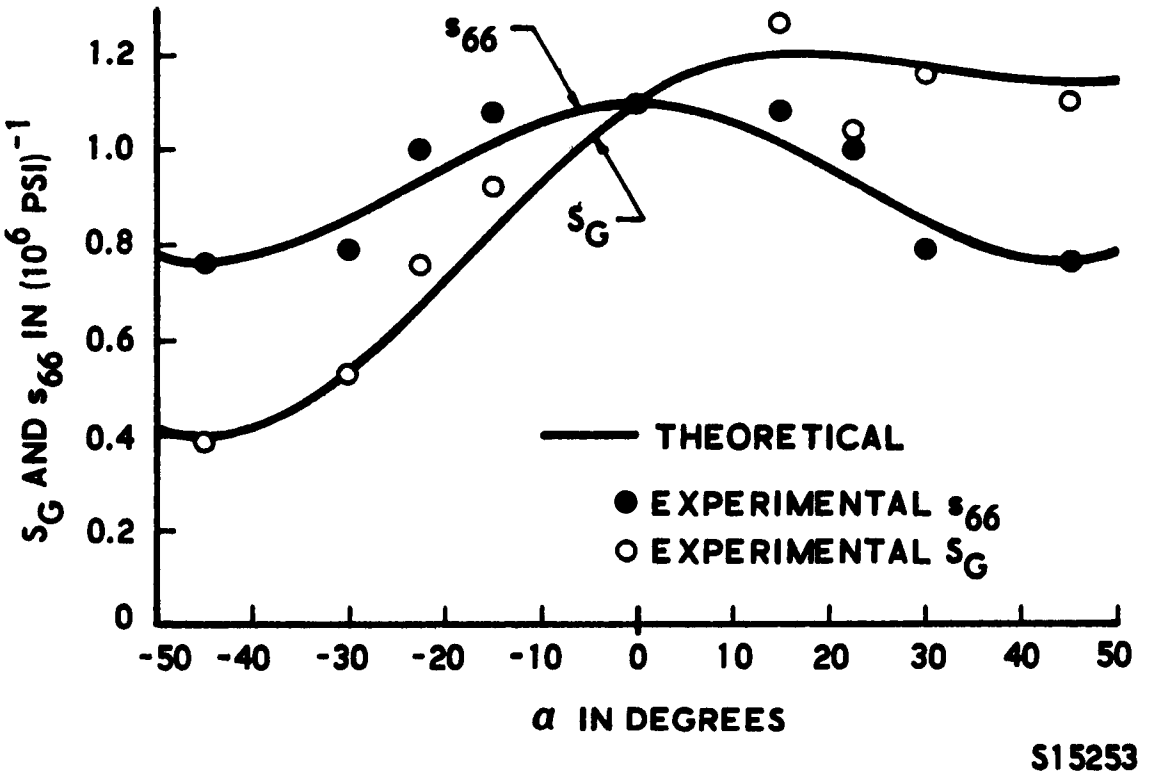

FIGURE A-4. S_G AND S_{66} - DATA VERSUS THEORY

CONCLUSIONS

It has been shown that the proposed method of determining the anisotropic elastic constants is easy to perform and yields reliable data. The special test fixture for the pure twisting test is extremely simple. Beyond this, no additional equipment, instrumentation, and strain gages are required. It has also been shown that independent check on the data can be readily obtained, e.g., bending of 90°-beams, and twisting of plates with orientations other than 0° and 45°. It should be pointed out that bending of beams other than 0° or 90° does not yield reliable data on s_{11} because s_{16} is not zero. The non-vanishing s_{16} induces shear strain which causes the beam to twist. The task of separating the deflection from twisting of a beam under the action of pure bending is not easy.

Test specimens for the proposed method must be flat plates. The measured data are applicable to anisotropic shells if they are made of the same material as the plates. To obtain the elastic constants of shells directly from shells involves a number of serious experimental difficulties. It is more advisable to determine the constants from plates with similar material as the shell and then make limited number of tests on the shell for checking purposes only.

REFERENCES

1. M. Bergstrasser, "Bestimmung der beiden elastischen Konstanten von plattenformigen Korpern," Zeitschrift fur Technische Physik, Vol. 8, 1927, pp 355-357.

2. R. F. S. Hearmon and E. H. Adams, "The Bending and Twisting of Anisotropic Plates," British Journal Applied Physics, Vol. 3, 1952, pp 150-156.

3. R. K. Witt, W. H. Hoppmann, II, and R. S. Buxbaum, "Determination of Elastic Constants of Orthotropic Materials, with special reference to laminates," ASTM Bulletin #194, 1953, pp 53-57.

APPENDIX B

The objective of the tests reported herin was to determine the modulus of elasticity in tension of composite media in which the matrix material was ascertained to be continuous, as opposed to composite media, such as glass reinforced plastic, in which individual elements of the reinforcement are in conjunction to various degrees.

To obtain the tensile modulus of transversely reinforced, continuous, matrix plastics, a specially designed specimen was necessary. A casting mold was fabricated as described in Table I. This mold allowed epoxy castings to be made which were reinforced 10 or 20 percent by volume with steel rods. Table I lists the materials and procedures employed in preparing and testing specimens of three epoxy resin systems reinforced 0, 10, and 20 percent by volume. I was found that normal machining (mill work) methods produced cracks near the steel reinforcement, and specimens were prepared by the less precise means of sawing and grinding.

Table II lists the modulus of elasticity of several reinforced and nonreinforced tensile specimens. Several autographically recorded stress/strain curves were obtained for each specimen. Care was taken not to fatigue the specimen. The estimated accuracy of the results is $\pm$ 10 percent, larger than the normal $\pm$ 5 percent testing error. This is caused by such reasons as undetected cracks and variations in specimen configuration and cross-sectional area.

TABLE I

MATERIALS AND PROCEDURES EMPLOYED IN FABRICATING TENSILE SPECIMENS

I. MATERIALS

Resin: Epon 828 epoxy resin (Shell Chemical Company)

Catalysts:

1. Metaphenylene diamine (MPD; C1 catalyst)
2. Boron flouride monoethylamine complex (BF3-400)
3. Hexahydrophthalic Anhydride (HHPA)
4. N,N - dimethyl benzlamine (DMBA)

Reinforcement: 1/16 inch diameter mild steel, copper clad welding rod.

II. CASTING MOLD DESCRIPTION

Mold cavity = 4 x 4 x 1 inch. Sides bolted to bottom plate. Two opposing sides perforated with 1/16-inch diameter holes to accommodate reinforcing rods. Each of the two opposing sides had 5 parallel rows holes, 1/8-inch apart center to center. The rows were 1/8-inch apart center to center, and the second and fourth rows were offset 1/16-inch from the others.

III. CASTING PROCEDURES

A. Prepare welding rods for casting by removing copper clad with HC1 acid, smut with HNO_3 acid, rinsing in distilled water, and drying with a clean cloth.

TABLE I (Continued)

B. Prepare mold with suitable release agent and insert rods in desired pattern, avoiding contact with release agent.

C. Fill mold with one of the following resin mixes (all components preheated to 160°F prior to mixing):

1. Epon 828 with 80 parts per hundred by weight (phr) HHPA and 0.8 phr DMBA.
2. Epon 828 with 13.5 phr MPD.
3. Epon 828 with 3 phr BF3-400.

D. Cure Cycles:

1. Epon 828/HHPA: 1/2 hour at 150°F and 4 hours at 225°F.
2. Epon 828/MPD: 4 hours at 150°F, one hour at 225°F and 2 hours at 350°F.
3. Epon 828/BF_3-400: 14 hours at 180°F, 6 hours at 200°F and 4 hours at 250°F.

IV. SPECIMEN PREPARATION

Saw, machine, and/or grind specimens to form tensile specimens with a 2-inch gage length.

V. TESTING PROCEDURE:

A. Bond doublers to gripped ends of each specimen with Eastman 910 adhesive.

TABLE I (Continued)

B. Using an Instron test machine and a Baldwin extensometer with 2-inch gage length, obtain the tensile modulus of each specimen as follows:

1. Set crosshead speed at 0.02-inch/min.
2. Load specimen to about 100 pounds while autographically recording the stress-strain curve at 1000 magnification. Unload specimen and repeat several times.
3. Obtain the slope of the initial straight-line portion of each curve.
4. Calculate modulus of elasticity in tension for each specimen as follows:

$$\text{Tensile Mod. (psi)} = \frac{\text{Avg. Slope (lb/in)}}{\text{Cross-section (in}^2\text{)}}$$

TABLE II

MODULUS OF ELASTICITY IN TENSION OF VARIOUS MILD STEEL REINFORCED AND NON-REINFORCED EPOXY SPECIMENS (TEST TEMPERATURE = 75°F)

Specimen Number	Casting Number	Reinforcement (Percent by Volume)	Rows of Reinforcement	Specimen Configuration*	Cross Section ($in.^2$)	Modulus of Elasticity In Tension (psi)
Epon 828/HHPA:						
1	2	0	0	Necked	0.157	472,000
2	2	0	0	Necked	0.115	455,000
					Average..	463,000
3	9	9.2	2**	Straight Bar	0.110	514,500
4	3	20.8	5	Straight Bar	0.235	756,000
4	3	21.3	3	Necked	0.135	795,000
5	3	19.7	3	Necked	0.146	698,000
Epon 828/MPD Catalyst:						
6	8	0	0	Necked	0.092	430,000
7	8	20.9	3	Necked	0.137	630,000
Epon 828/BF_3:						
8	4	0	0	Straight Bar	0.144	539,000
9	4	22.5	3	Necked	0.127	753,000

*Necked specimens were "dogbone" shaped with a 2-inch long straight portion.

**Two rows of reinforcement 1/4-inch apart, (for 20-percent specimens, the rows were 1/8-inch apart).

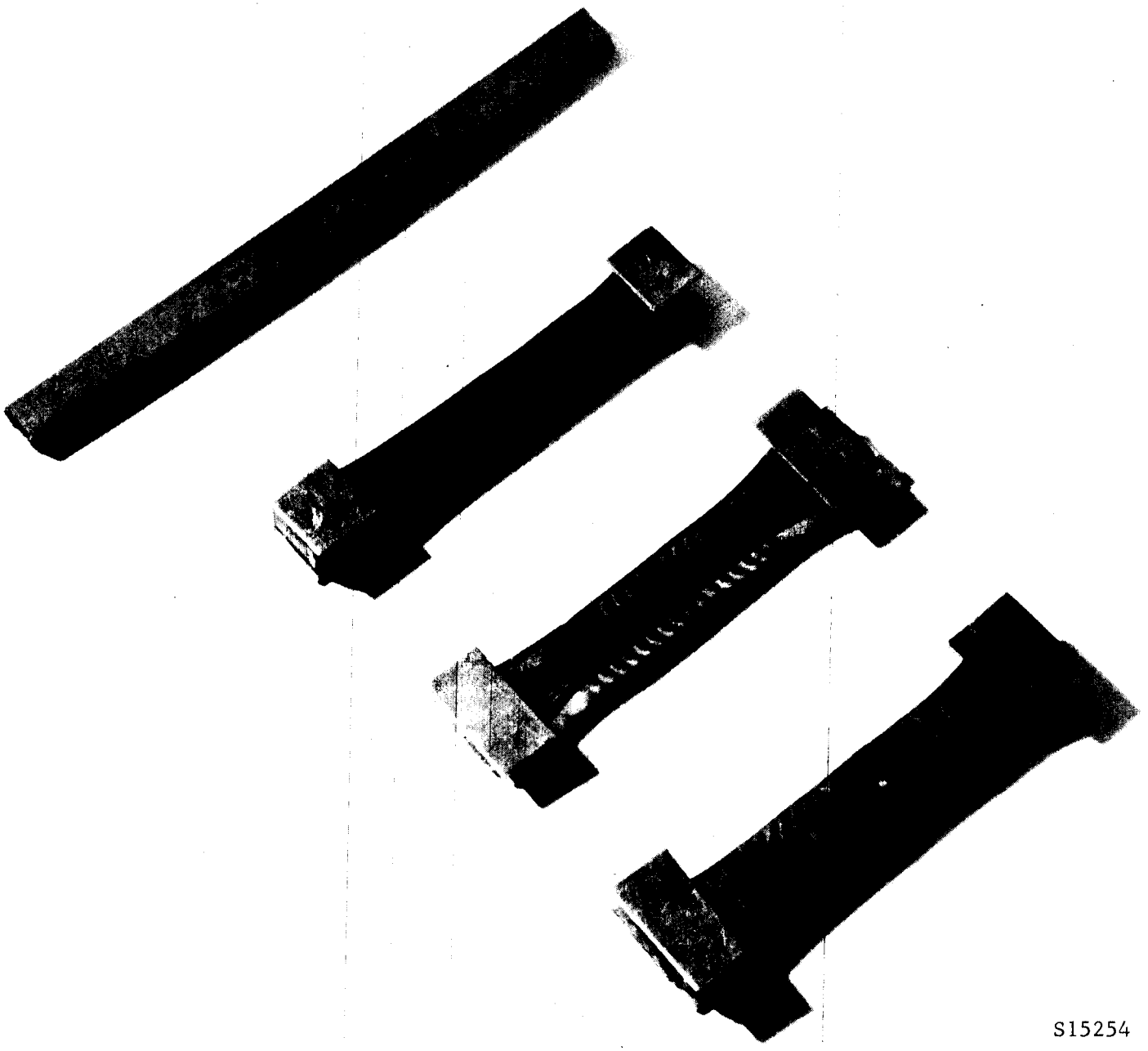

FIGURE B-1. STEEL - EPOXY SPECIMENS